Calculation of photoemission from atoms subject to intense laser fields

Jeffrey L. Krause, Kenneth J. Schafer, and Kenneth C. Kulander
Physics Department, Lawrence Livermore National Laboratory, Livermore, California 94550
(Received 18 January 1991; revised manuscript received 8 November 1991)

We use a nonperturbative method to solve the time-dependent Schrödinger equation for an electronic state of an atom subject to a very intense ($> 10^{13}$ W/cm^2) laser. The oscillating, time-dependent dipole induced by the laser serves as a source for the photoemission. Calculations of single-atom photospectra reveal peaks at the odd harmonics of the incident laser field superimposed on a broad continuous background. We discuss a series of calculations for the hydrogen atom and a short-range Yukawa potential containing a variable number of bound states. At intensities up to a few times 10^{13} W/cm^2 at 1064 nm, we achieve stable, converged spectra that agree very well with previously published results. As the intensity increases to 10^{14} W/cm^2, the ionization rate increases to about 1% of the laser frequency, and converged results become extremely difficult to obtain, even for impractically large integration volumes. These difficulties are caused by a rising background due to electron density far from the nucleus and the increasing importance of the interaction of the wave function with the edges of the grid. We discuss the implications of our findings for calculations at high intensity and suggest alternative ways to calculate harmonic emission rates in the strong-ionization regime.

PACS number(s): 42.50.Hz, 32.80.Rm

I. INTRODUCTION

Current laser systems are capable of developing field strengths comparable to or greater than the binding energy of a valence electron to an atom or molecule. The exceedingly nonlinear interaction of such lasers with matter has led to the discovery of a number of unusual and unexpected results. Perhaps the most spectacular of these is optical harmonic generation (OHG). In this process, a target atom X absorbs q photons and emits one photon of q times the energy of the incident photon

$$X + q\gamma(\hbar\omega_0) \rightarrow X + \gamma'(q\hbar\omega_0) , \quad (1)$$

where ω_0 is the laser frequency and X may, in general, become multiply ionized during the course of the laser pulse. While nonlinear mixing of laser frequencies in gases has been known for many years, harmonics have now been observed to very high order. Experiments by McPherson *et al.* [1], for example, at an intensity of 10^{15}–10^{16} W/cm^2, observed photons at 14 nm, or 85 eV, corresponding to the 17th harmonic of the KrF fundamental. L'Huillier *et al.* [2], using a picosecond Nd-glass laser at an intensity of $\sim 5\times 10^{14}$ W/cm^2 in neon, detected harmonics up to the 53rd, and hence photons at 20 nm, or 62 eV. Recently, Sarukura *et al.* [3] observed the 25th harmonic (< 10 nm) of KrF in neon. Observation of OHG requires laser illumination and proper phase-matching conditions. The emitted harmonics are coherent [4], and have peak spectral brightness at least comparable to conventional synchrotron sources [5], so OHG has the potential to become a useful laboratory source of vacuum ultraviolet to x-ray photons.

Optical harmonic generation is one type of nonlinear response of matter to radiation, and its basic physics is reasonably well understood [4–8]. A laser field induces a time-varying dipole moment in an atom or molecule. In a weak field, the dipole moment is strongly dominated by the laser frequency, ω_0. In a strong field, the dipole moment develops frequency components at multiples (harmonics) of the laser frequency, $q\omega_0$, which can act as sources of radiation. The even harmonics are forbidden by parity conservation in a medium with inversion symmetry, so the optical harmonic spectrum consists of a series of peaks centered at odd multiples of the laser frequency.

The low-order harmonics can be viewed as arising from multiphoton transitions to, and subsequent radiation from, virtual bound levels. The high-order harmonics result from photon absorption above the ionization threshold, and can be described in terms of a dressed continuum [8]. A strong relationship has thus been predicted between the peaks seen in above-threshold-ionization (ATI) spectra and harmonic spectra [9]. These two processes cannot be compared in a single experiment because ATI experiments must be done at low gas pressure to minimize atomic collisions and space-charge distortion of the energy distribution, while OHG experiments are performed at much higher pressure, due to the coherent N^2 enhancement of the harmonic signal (where N is the number of atoms producing the observed harmonic).

Calculating the optical response of materials to intense laser fields presents a severe challenge. Perturbative methods, which rely on expanding the nonlinear response of an electron to an electric field in a series of susceptibilities, fail at high intensity when the susceptibilities themselves become intensity dependent. Several schemes have been developed to model the emission from atoms in the nonperturbative regime. Prominent among these are methods employing Floquet theory [10], dressed states [11], classical trajectories [12], and direct numerical in-

tegration of the time-dependent Schrödinger equation [9,13–16].

In this paper we present the results of a detailed investigation of the applicability of time-dependent numerical techniques to the study of OHG. Although the methods and conclusions we present are relevant to OHG in any gaseous medium, we focus here on results for the hydrogen atom, which can be treated exactly with our approach. By solving the time-dependent Schrödinger equation directly, we treat the intra-atomic forces and the electron-laser interactions explicitly, and need make no assumptions about their relative magnitudes. In an effort to better understand the dynamics of harmonic generation, we examine the intensity dependence of the harmonics as well as how the electronic structure of the atom affects the spectra. We demonstrate that when the atom ionizes appreciably during the course of an optical cycle, obtaining numerically converged spectra (that is, spectra which do not change as the parameters of the calculation are varied) is very difficult. This is particularly true when the length form of the dipole moment is used. Therefore, we have also investigated two alternative forms of the dipole, which give a larger weight to the dynamics near the nucleus.

Experimental harmonic spectra, and spectra calculated from time-dependent quantum methods and classical trajectories, consist of a series of peaks superimposed on a broad, continuous background. (Floquet calculations that require the field to be exactly periodic cannot calculate the response of the atom at nonharmonic frequencies, and so do not address the issue of the background.) Calculations on inadequate (i.e., too small) spatial grids cannot accurately characterize the bound excited states and thus greatly underestimate the strength of the background emission. Small grid calculations may also predict inaccurate harmonic intensities. We will show that the magnitude of the background depends very strongly on the presence of a set of bound excited states of the atom. The background is time dependent, and can be very sensitive to both the integration parameters of the calculation and the pulse shape of the laser. When the atom is ionizing rapidly, the ionizing portion of the wave function interferes with the part of the wave function responsible for the harmonic and causes significant variations in the harmonic intensities with comparatively small changes in the parameters of the calculation. However, at intensities up to a few times 10^{13} W/cm^2 at 1064 nm, with an adequate representation of the low-lying states and careful attention to the calculational details, numerically converged harmonic intensities can be obtained.

In this paper, we discuss in detail calculations of the photoemission from a hydrogen atom in a 1064-nm laser field with a peak intensity of 2×10^{13} W/cm^2. At this intensity, we obtain an ionization rate of $\sim4\times10^{7}$ s^{-1}, which is in excellent agreement with the Floquet calculations of Potvliege and Shakeshaft [10], and is at least five orders of magnitude below the lowest-order perturbation theory result [10]. Therefore, this is a regime well above that in which perturbation theory is valid, and one in which concepts based on field-free atomic states can be misleading. The ponderomotive shift of the ionization potential at 2×10^{13} is ~2 eV, which exceeds the photon energy, so any excited "states" that exist under these conditions will be very strongly mixed, or dressed, by the field. With our method, however, this intensity is fairly low in the sense that very little of the atom ionizes during a single optical cycle. We show that when the intensity is increased to 1×10^{14} W/cm^2 at 1064 nm, the atom ionizes in less than a picosecond and a qualitative change in the dynamics occurs. Increased ionization causes the wave function to spread rapidly over large regions of space, which has both physical and computational implications. Obviously, rapid ionization occurs in all systems at high enough intensity. We illustrate how the difficulties encountered under such conditions affect the interpretation of calculations and experiments.

II. METHOD

The solution of the time-dependent Schrödinger equation can be efficiently realized by using a grid representation of the electronic wave function. This method has been described previously in other contexts [16–18], so here we concentrate only on the details particular to the calculation of optical harmonic spectra.

We consider the case of the hydrogen atom in a linearly polarized, classical laser field. The method proceeds by solving the time-dependent Schrödinger equation, which can be written in atomic units as

$$i\frac{\partial}{\partial t}\psi(\mathbf{r},t)=H(\mathbf{r},t)\psi(\mathbf{r},t)\ . \tag{2}$$

We expand the electronic wave function in spherical harmonics [17,18],

$$\psi(r,\theta,\phi,t)=\sum_{l=0}^{L}\sum_{m=-l}^{l}\frac{\Phi_{l,m}(r,t)}{r}Y_l^m(\theta,\phi)\ , \tag{3}$$

and discretize the resulting coupled equations on a radial grid between $r=0$ and R, with a maximum of L angular momentum channels. The azimuthal quantum number m is conserved because the laser is linearly polarized. All of the calculations presented in this paper begin in the $1s$ ground state, in which $m=0$. The choices of L, R, and the radial grid spacing are dictated by the vicissitudes of convergence. The discretized equations are derived variationally from a Lagrangian formulation that is equivalent to the Schrödinger representation, but allows us to explicitly consider the $r=0$ boundary. The Hamiltonian for this system is then

$$H=H_0+H_I(t)\ . \tag{4}$$

H_0^l is the atomic Hamiltonian,

$$H_0^l=-\frac{1}{2}\frac{d^2}{dr^2}+\frac{l(l+1)}{2r^2}-\frac{1}{r}\ , \tag{5}$$

and $H_I(t)$ is the atom-field interaction, given by

$$H_I(t)=-\varepsilon_0 f(t)z\sin(\omega_0 t)\ , \tag{6}$$

where we have assumed that the field is polarized along the $\hat{\mathbf{z}}$ direction. $f(t)$ is a slowly varying envelope func-

tion that models the intensity evolution of the laser field. The peak intensity is $c\varepsilon_0^2/(8\pi)$ in atomic units. Since the laser field couples only angular momentum channels with $l\pm1$, the Hamiltonian operator is tridiagonal in l, making it possible to integrate the resulting coupled equations very efficiently [19]. An alternative procedure [16], in which ψ is expanded in cylindrical, instead of spherical, coordinates was also tested. This method gives the same results, but requires a larger number of grid points.

Equation (2) is an initial-value problem, and requires as input the ground state of the atom on the grid. The ground state can be calculated in one of two ways, either by diagonalizing the field-free (discretized) Hamiltonian, or by integrating Eq. (2) in imaginary time in the absence of the field with an initial guess for the wave function [20,21]. For any reasonable starting function, the imaginary time propagation causes the trial function to relax to the ground state in a small number (~ 50) of integration steps. Both methods yield a wave function that is an eigenstate of the discretized Hamiltonian. If this procedure is not followed (if, for example, an eigenstate of the continuous Hamiltonian is used), nonphysical couplings between numerical eigenstates of the grid will be introduced, leading to spurious oscillations in the time-dependent wave function.

In the case of hydrogenic potentials, the wave function can be further improved by imposing a discrete form of the virial theorem. One way to do this is to spread the positive nuclear charge uniformly over an area equal to about one grid spacing. This introduces an additional potential at the $r=0$ boundary which, when properly chosen, results in a ground-state wave function that obeys the virial theorem to very high accuracy. In addition, this procedure produces a grid eigenstate that has a greatly reduced discrepancy between the discretized and the analytic wave functions.

The single-atom emission spectrum can be determined from the time-varying, induced dipole of the excited system [6]. The length form of the dipole can be calculated from the time-dependent wave function as

$$d(t)=\int d\mathbf{r}\,\psi^*(\mathbf{r},t)z\psi(\mathbf{r},t)\ . \tag{7}$$

Note that this form is independent of the gauge ($\mathbf{A}\cdot\mathbf{p}$ or $\mathbf{E}\cdot\mathbf{r}$) used to calculate $\psi(\mathbf{r},t)$. The harmonic spectrum is proportional to the square of the Fourier transform of $\langle d(t)\rangle$,

$$\sigma(\omega)\propto|d(\omega)|^2=\left|\frac{1}{T_2-T_1}\int_{T_1}^{T_2}dt\,e^{-i\omega t}d(t)\right|^2\ . \tag{8}$$

To determine the power emitted in a given harmonic, $|d(\omega)|^2$ in Eq. (8) should be multiplied by ω^3. In an effort to minimize the complications caused by a time-varying pulse, and to focus on the emission of an atom subject to a particular intensity, we use a pulse consisting of a linear (or $\sin^2$) ramp of the electric field for 2–10 optical cycles, followed by 15–20 additional cycles at a constant intensity. To generate the spectrum, we Fourier transform only the final 5–10 cycles. By this time, the transients induced by the ramp have decayed, and the spectrum depends only on the laser frequency and intensity. This method is a reasonable approximation to the usual case of a laser pulse consisting of hundreds or thousands of optical cycles at approximately the same intensity. For very short pulses (<100 fs), the emission spectrum should be obtained from the transform of the induced dipole over the entire pulse. We note that the n-cycle Fourier transform is performed only at frequencies $\omega=k\omega_0/n$, where k is an integer, to avoid introducing aliasing errors due to a finite time series.

III. RESULTS

Figure 1 shows the time-dependent dipole induced by a pulse that increased over 5 optical cycles, and then was held constant for the next 15 cycles. This calculation used a photon wavelength of 1064 nm, the fundamental of a Nd:YAG laser (where YAG denotes yttrium aluminum garnet), a peak intensity of 2×10^{13} W/cm^2, and was performed on a grid with a maximum radius of $225a_0$, and a maximum l of 48. The integration time step was 1/800 of an optical cycle and the grid spacing was $0.25a_0$. After each time step the wave function was multiplied by a $\cos^{1/8}$ mask function that varied from 1 to 0 over a width of $50a_0$ at the outer radial boundary. The purpose of the mask function was to force the electron density to zero at the edge of the grid to prevent reflection of the wave function from the grid boundaries, as discussed below.

The absolute square of the Fourier transform of the calculated time-dependent dipole in Fig. 1 is proportional to the emission spectrum of a single atom in the field. Figure 2 shows the spectrum obtained from the last five optical cycles of the dipole in Fig. 1. Using too few cycles in the Fourier transform results in a noisy or poorly resolved spectrum, and choosing cycles too close to the ramp causes variations in the spectrum due to transients induced by the field gradient. At higher intensities, the transients decay very quickly, and the ramp becomes less important. The results in Figs. 1 and 2 are independent of the upper limit of the radial integration in Eq. (7) as long as it is at least $\sim 25a_0$. This indicates that the physi-

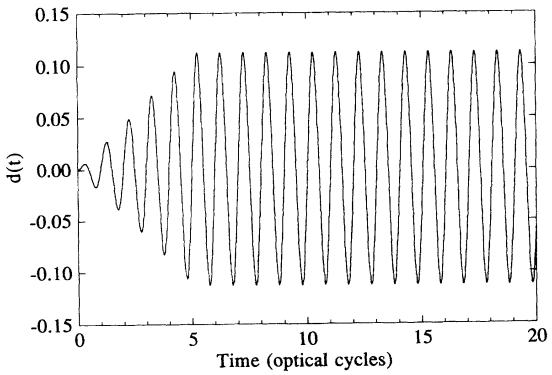

FIG. 1. Time-dependent dipole $\langle d(t)\rangle$ induced in a hydrogen atom by a 1064-nm laser pulse at 2×10^{13} W/cm^2. The field was ramped to its maximum intensity over 5 optical cycles, and held constant for 15 additional cycles.

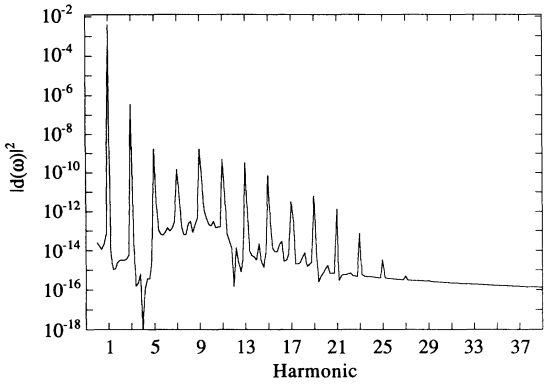

FIG. 2. Harmonic spectrum $|d(\omega)|^2$ obtained from a Fourier transform of the last 5 optical cycles of the time-dependent dipole in Fig. 1.

cally significant excitation dynamics responsible for the photoemission at this intensity take place near the atom.

The photoemission in Fig. 2 consists of a series of narrow peaks at odd frequencies of the fundamental, and a broad, significantly weaker background that reaches a maximum near the energies of the field-free Rydberg states. The widths of the harmonic peaks correspond to the inverse of the period over which the induced dipole was transformed. If the ionization rate were fast on this time scale, the peaks would be further broadened. At 2×10^{13} W/cm^2, and 1064 nm, 14 photons are required to ionize the atom. As seen in Fig. 2, the harmonic emission extends well beyond the (Stark-shifted) ionization threshold. The harmonic intensities are converged with respect to such integration parameters as the time step, grid spacing, and box size, and do not change if the ramp parameters or absorbing boundary are varied over a reasonable range.

The spectrum in Fig. 2 is stable at the frequencies of the odd harmonics ($\omega=q\omega_0$, where $q=1,3,5,\ldots$). By stable we mean that both the magnitude and phase of $d(q\omega_0)$ are independent of the integration parameters, as well as which cycles after the transient period are included in the Fourier transform. At nonharmonic frequencies, the phase of $d(\omega)$ changes from cycle to cycle. The amplitudes of the weak background features in the Rydberg region differ somewhat depending on which cycles are Fourier transformed, but do not change qualitatively.

As we mentioned previously, harmonic generation is a coherent process, and therefore the harmonics are enhanced by a factor of N^2 in the experiments and in calculations including the effects of phase matching [7]. The background radiation in our calculated spectra does not have a constant phase from cycle to cycle, and so is incoherent and will not phase match over a macroscopic distance. Since a single-atom spectrum, such as the one in Fig. 2, does not include the effects of phase matching, it tends to obscure the difference between the coherent emission at the odd harmonic frequencies, and the incoherent emission at all other frequencies, and hence greatly overestimates the importance of the background. In a single-atom calculation, however, there is no way to separate the two contributions to the dipole. This presents no problem when the harmonic intensities are well separated from the background, since it is clear at which frequencies the harmonic photoemission occurs. In general, at least for the lower-order harmonics, an estimate of the harmonic conversion efficiency can be reliably determined from a single-atom spectrum.

We would like to point out that the background in the experiments, which is clearly observed, arises predominantly from sources not included in the calculations. For example, the experimental background contains many closely spaced fluorescence lines caused by emission after the pulse is over, on a time scale very long compared to the harmonic emission [5]. This component of the background can be removed by performing time-resolved experiments [22].

The harmonic intensities in Fig. 2 agree very well with the previously published results of Potvliege and Shakeshaft [10], as shown in Fig. 3 at 2×10^{13} W/cm^2, and wavelengths of 532 and 1064 nm. This agreement is gratifying because the Floquet ansatz is expected to be very good at the intensity and wavelengths of the figure. We have also calculated emission spectra with an equivalent velocity gauge formulation, in which the harmonic spectrum is obtained from the current, rather than the time-dependent dipole, and obtained the same results.

Calculations employing grids as large as those used to produce the results of Figs. 1–3 are fairly demanding computationally, taking on the order of 10–20 min on a supercomputer. Our code is essentially completely vectorized, and linear in the number of grid points. It propagates the wave function at a rate of over one million space-time points per second on a Cray Y-MP computer. Although this is quite efficient, it would be very desirable to reduce the size of the grid significantly, yet still determine accurate photoemission probabilities.

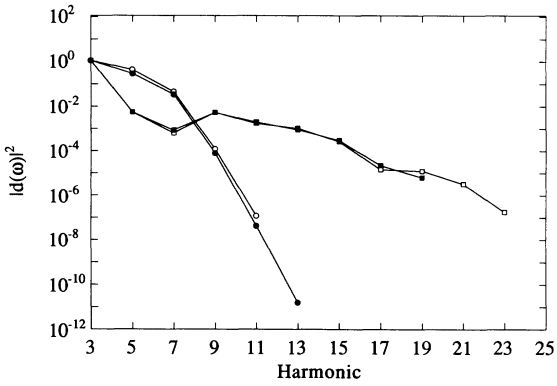

FIG. 3. Comparison of harmonic intensities as calculated in this work with previously published results using a method based on Floquet theory (Ref. [10]). The laser intensity is 2×10^{13} W/cm^2, at wavelengths of 1064 nm (filled squares, this work; open squares, Ref. [10]) and 532 nm (filled circles, this work; open circles, Ref. [10]). The first harmonics have been omitted from the plot, and the intensities have been normalized at the third harmonic. Note that, as published, the Floquet results contain a factor of ω^3, which has been removed in this figure.

The ability to use small grids depends critically on the range over which the relevant dynamics occurs. In a photoionization problem, the extent of the electronic wave function increases without limit as time increases. At any finite time, however, the extent of the wave function is finite. Since an electron absorbs photons primarily near the nucleus, and since an electron that absorbs enough photons to ionize never returns to the nucleus, calculations of ionization rates can be accurately realized on relatively small grids [16]. In contrast, calculating ATI spectra requires knowledge of the entire final-state wave function, and hence demands grids large enough to contain all, or most, of the ionizing wave function [23]. Our experience indicates that calculations of OHG require grids intermediate in size between the extremes of ionization rates and ATI.

Figure 4(a) shows a harmonic spectrum for the hydrogen atom, at a laser intensity of 2×10^{13} W/cm^2, as calculated on a $50a_0$ grid with an absorbing boundary similar to that used in our ionization rate calculations (a width of $\sim10a_0$ [16]. Since the quiver motion of the electron at this intensity is only about $13a_0$, it would seem that $50a_0$ would be adequate to characterize the dynamics. However, when Fig. 4(a) is compared to the converged spectrum of Fig. 2, which is reproduced in Fig. 4(b), two striking differences are immediately revealed. The small grid spectrum has a *much* lower background, and many more harmonics than the converged spectrum. The harmonic intensities on the small grid, though generally correct to within an order of magnitude, differ from the converged values and are very sensitive to variations in the integration parameters, as well as the form and strength of the absorbing boundary.

The additional, spurious harmonics seen in Fig. 4(a) but not in the converged spectrum of Fig. 4(b) are caused by reflection from the grid boundary. When flux reaches the boundary of the grid, the instantaneous electric field is driving it predominantly outward, along the axis of polarization. If the flux reflects elastically from the boundary, it is accelerated towards the nucleus when the field reverses its direction during the next half of the optical cycle. This causes the reflected flux to have a much higher velocity when it subsequently rescatters from the nucleus. Even a very small amplitude of energetic flux is sufficient to cause spurious high harmonics such as those seen in Fig. 4(a). Reflection can be minimized by using a very soft (apotropaic) mask function, but cannot be completely eliminated when the wave function is interacting with the edge of the grid. We have tested many different functional forms for the absorber, including Gaussians and exponentials of varying widths and strengths, linear functions, and several powers of the cosine. We find that a broad, smooth function, such as $\cos^{1/8}$, is the most effective, while a function with a kink, such as linear, is the worst. The main reason for the sensitivity to the form of the mask function is that reflection tends to occur at the boundary between the grid and the absorber. With any reasonable mask, essentially no flux actually reaches the edge of the grid, so the part of the absorber that is most critical is the leading edge, which should be as smooth as possible. We have also tested the use of a complex absorbing potential instead of a mask, and found that the two methods are basically equivalent. The mask has the advantage that it requires less computer memory, since the potential is real, rather than complex.

With boundary conditions that force the wave function to zero at a finite distance from the nucleus, no state is truly bound, but the tunneling lifetime of many states is long enough for them to behave as if they were bound. States near the ionization limit are strongly affected by the absorber, which effectively lowers the ionization potential. These states are presumably not important in calculations of the ionization rate because excitation to such energies at high intensity, where the states are significantly shifted and broadened, is followed by facile transitions into the continuum. Similarly, the very-high-lying states have little influence on the photoemission, since electrons excited to such states are either ionized immediately, or cannot reach the outer turning point of the potential and return to regions near the nucleus on the time scale of the laser pulse. The low-lying excited states, however, appear to be strongly involved in the creation of the harmonics, as well as the background radiation.

The reduction in the magnitude of the background on a small grid seen in Fig. 4(a) is quite surprising, and appears to be related to the lower number of effectively bound states in the problem. To test this hypothesis, we

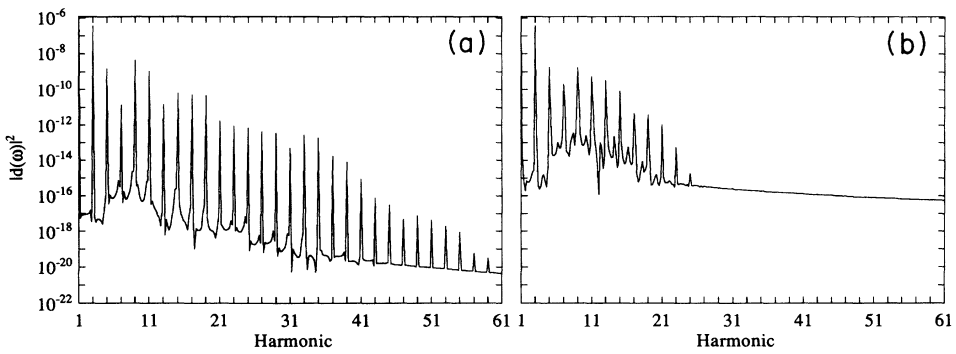

FIG. 4. Harmonic spectra at 2×10^{13} W/cm^2 and 1064 nm, calculated on radial grids of (left) $50a_0$ and (right) $250a_0$.

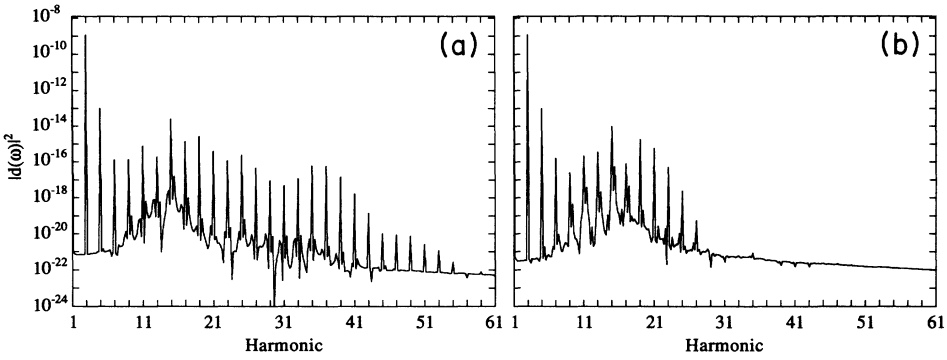

FIG. 5. Same as in Fig. 4, using a Yukawa potential, rather than the hydrogenic Coulomb potential. The Yukawa parameters were adjusted so that the potential supported only one bound state, at $0.5a_0$ below the (field-free) ionization threshold.

performed a series of calculations with a Yukawa (or screened Coulomb) potential of the form,

$$V(r)=Z'\frac{e^{-\alpha r}}{r}\ , \tag{9}$$

in which we adjusted α to change the number of bound states in the potential. Because the number and intensity of the harmonics at a given laser intensity depends strongly on the ionization potential, we also varied Z' to maintain a constant (field-free) ionization potential of 0.5 a.u.

Figure 5 shows the harmonic spectra for a Yukawa potential with one bound state on a $50a_0$ grid compared to the spectra obtained on a $250a_0$ grid. As in the calculation with the Coulomb potential, the spectra on the smaller grid has additional harmonics caused by reflection. In contrast to the Coulomb case, however, the background levels in Figs. 5(a) and 5(b) are nearly the same. Comparing the spectra from the two potentials (Fig. 6), we see that the harmonic intensities, as well as the background intensities, are significantly reduced in magnitude in the Yukawa potential. The ionization rate for the Yukawa potential is also reduced by a factor of about 100 compared to the Coulomb potential, due to the absence of resonant, or near-resonant, contributions to ionization by the excited states. Note, though, that the two spectra in Fig. 6 have about the same number of harmonic peaks. This may be consistent with the recent suggestion that the number of harmonics is related to the ratio of a mean Rabi frequency to the laser frequency [24]. In the one-state Yukawa potential, however, the definition of a Rabi frequency is somewhat unclear.

As $\alpha\rightarrow 0$, and $Z'\rightarrow 1.0$, the ionization rate and the background levels of the spectra calculated with the Yukawa potential increase smoothly to the Coulomb limit. At 2×10^{13} W/cm^2, with α such that the Yukawa potential contains 4 (field-free) bound $l=0$ states, the Yukawa spectrum becomes identical to the Coulomb spectrum. The sensitivity of the background to the number of bound state suggests that a major component of the background is due to population of excited states by the laser pulse, and subsequent incoherent beating, or "Raman-like" transitions among them. A similar mechanism has been suggested previously to explain supercontinuum emission in gases [25]. The importance of such transitions also accounts for the dependence of the background on which cycles are included in the Fourier transform, because the excited-state population continues to evolve in time throughout the laser pulse. We note also that the general shape of the background in the Yukawa spectrum is very similar to that in the hydrogen atom, but is much weaker and shifted to higher energy. In the Coulomb po-

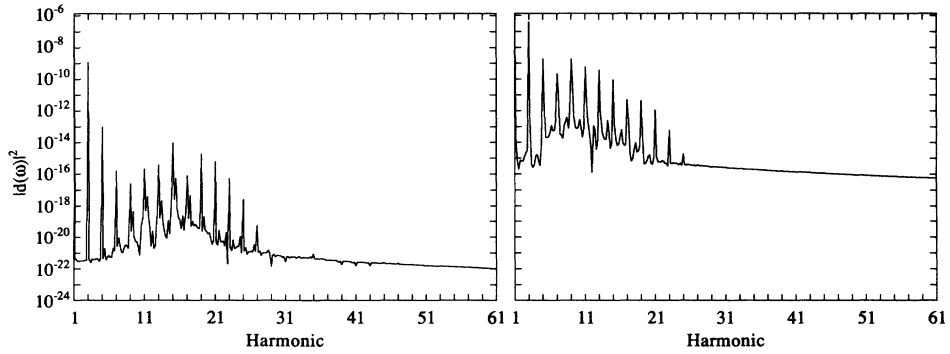

FIG. 6. Comparison of harmonic spectra for (right) the Coulomb potential and (left) the 1-state Yukawa potential at 2×10^{13} W/cm^2 and 1064 nm. Both spectra were calculated on a radial grid of $250a_0$.

tential, the broad peak in the background is presumably related to the increased density of states near threshold. In the Yukawa potential, the peak is shifted into the continuum, where the oscillator strength of this system is concentrated, and is much more a property of continuum to continuum transitions. The background in all of the cases that we have studied decreases asymptotically as $1/\omega^2$.

The importance of the density and energies of the low-lying bound states on the grid, along with the near impossibility of completely preventing reflection from the grid boundaries, explains in part the sensitivity of the harmonic spectra calculated on small grids at low intensity. Fairly small variations in the integration parameters are sufficient to shift the energy levels, and hence to cause significant changes in the excitation dynamics. We often find that one or two harmonics are especially sensitive. Such behavior is a signature of resonant interference, as discussed below.

We have illustrated that with some care converged harmonic spectra can be calculated on moderate grids at an intensity of 2×10^{13} W/cm^2. However, for hydrogen at 1064 nm, this is a fairly low intensity, in the sense that most of the electron density remains relatively close to the nucleus, and the ionization rate is quite low, about 10^{-7} per optical cycle. As the intensity increases, several factors conspire to make the physics more interesting, and to complicate the calculations as well as the interpretation of the results.

Figure 7 shows the ionization rate of the hydrogen atom as a function of laser intensity at 1064 nm. These rates were determined by calculating the decay of the norm of the wave function on the grid as a function of time. Rates obtained by this method do not differ significantly from those calculated by monitoring the decay of the ground state, except at very low intensity. As can be seen in the figure, the ionization rate first increases rapidly, and then begins to saturate. As the intensity increases, the ionization rate becomes quite smooth. This is a characteristic of tunneling ionization, which occurs when the Keldysh parameter [26],

$$\gamma^2=\frac{2\omega_0^2 I_0}{I} \tag{10}$$

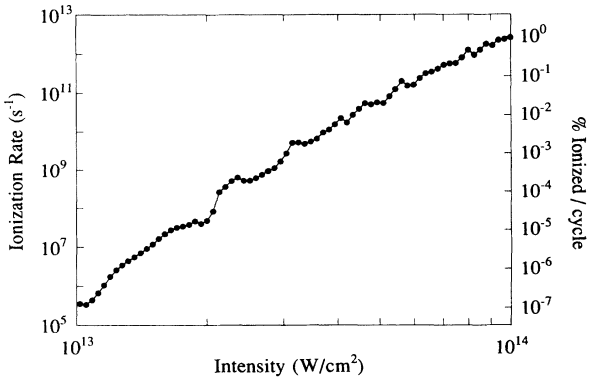

FIG. 7. Ionization rate (in s^{-1} and % per optical cycle) of a hydrogen atom at 1064 nm as a function of the laser intensity.

is less than, or on the order of, 1. In Eq. (10), I_0 is the field-free ionization potential, I is the laser intensity, and ω_0 is the laser frequency. At 1064 nm, γ^2 equals 6.4 at 1×10^{13} W/cm^2, and decreases to 0.64 at 1×10^{14} W/cm^{20}, which is clearly in the tunneling regime. By 1×10^{14} W/cm^2, the ac Stark shift of the continuum, which is given by the ponderomotive energy

$$E_p=\frac{I}{4\omega_0^2}\ , \tag{11}$$

is about 11 eV, so most of the bound states have been shifted to very high energy, and the role of resonant excitation is greatly reduced.

By the highest intensity shown in Fig. 7, the atom ionizes in less than a picosecond, which corresponds to about 1% of the atom per optical cycle. We have found that this parameter, the amount of ionization per cycle, is the factor that determines whether the ionization rate is "high" or "low" in our calculations. As the ionization rate increases, the spatial extent of the wave function also increases, because the photoelectrons are emitted with higher energy (via ATI). By 10^{14} W/cm^2, the size of the grid in r and l that would be required to completely contain the ionizing wave function is enormous. Since the Hamiltonian in the length gauge is proportional to both the magnitude of the electric field and the maximum extent of the grid, as either I or R increases the time step must decrease. As the wave function spreads in r, more l's are necessary as well, because the wave function tends to elongate along the direction of polarization. These factors mean that calculations at "high" intensities require greatly increased resources, both in memory and CPU time. As a practical matter, at high intensity it is not feasible to perform calculations in which the grid is large enough to prevent the wave function from reaching the boundaries of the grid, and in which the time step is small enough to assure convergence. For example, at 1×10^{14} W/cm^2, a radial grid of $2000a_0$, $L=120$ and 2000 steps per optical cycle is still insufficient to converge the harmonic intensities to better than one to two orders of magnitude. Such a grid is already unphysically large, because the interatomic spacing at the tens of torr pressure in the experiments is only about $200a_0$. If the important dynamics really occurs on scales much larger than the interatomic spacing, calculations that do not include the atom-atom interactions would be meaningless. We do not expect this to be the case, however, and will show that the critical spatial volume is in reality much closer to the atom.

When the wave function is interacting strongly with the edge of the grid, the results become very sensitive to the parameters of the calculation. One contribution to this sensitivity can be discerned by examining the intensity dependence of the harmonics. Figure 8(a) shows harmonic intensities for the hydrogen atom at 1064 nm as a function of the laser intensity for harmonics 1, 3, and 5. All three of these harmonics begin in the perturbative regime, where their intensity dependence is well fit by a straight line. The slopes of these lines give the first-, third, and fifth-order susceptibilities. Our calculated values for these susceptibilities, along with the first-order

corrections to them, are shown in Table I, where they are compared to the perturbative calculations of Pan and co-workers [27]. The agreement is excellent.

At some intensity, about 8×10^{13} W/cm^2 for the first harmonic, 6×10^{13} for the third and 2×10^{13} W/cm^2 for the fifth, perturbation theory breaks down. The harmonics begin to scale with a dependence less than I^q, where q is the harmonic order, and start to develop resonance structure. The intensity at which perturbation theory becomes invalid decreases with increasing harmonic order, again in agreement with the calculations of Pan and co-workers [27]. This behavior is seen even more clearly, in Fig. 8(b), which shows the intensity dependence of harmonics, 7, 9, and 11. These harmonics are nonperturbative over the entire intensity range of the calculations. At lower intensity, the harmonics have fairly broad, well-spaced resonance structures that can probably be associated with individual atomic states Stark shifting through resonance, and should be observable experimentally. At higher intensity, the resonances become much more closely spaced, and the harmonics have roughly the same overall scaling with intensity. This constant scaling signifies the formation of a plateau in the harmonic spectra. At very high intensity, the resonances overlap, and the harmonic intensities oscillate rapidly. In this regime, harmonic generation is dominated by the interference of many excitation and ionization pathways, and in general the individual peaks cannot be associated with a particular atomic state. In fact, the atomic states have been broadened and shifted by the field to such an extent that the quantum numbers labeling the field-free atomic states are no longer meaningful. Comparing Fig. 8 to Fig. 7, we see that the harmonics are much more sensitive to this in-

TABLE I. First-, third-, and fifth-order susceptibilities χ_i, and their first-order corrections $\chi_i^{(2)}$, for the hydrogen atom at 1064 nm as calculated in this work, compared to the perturbative calculations of Pan and co-workers [27]. The numbers in square brackets denote powers of 10.

Susceptibility	This work	Ref. [27]
χ_1	4.550	4.550
χ_1	4.550	4.550
$\chi_1^{(2)}$	7.98[2]	8.96[2]
χ_3	2.81[2]	2.78[2]
$\chi_3^{(2)}$	1.97[5]	2.04[5]
χ_5	8.24[4]	9.03[4]
$\chi_5^{(2)}$	5.76[8]	2.51[8]

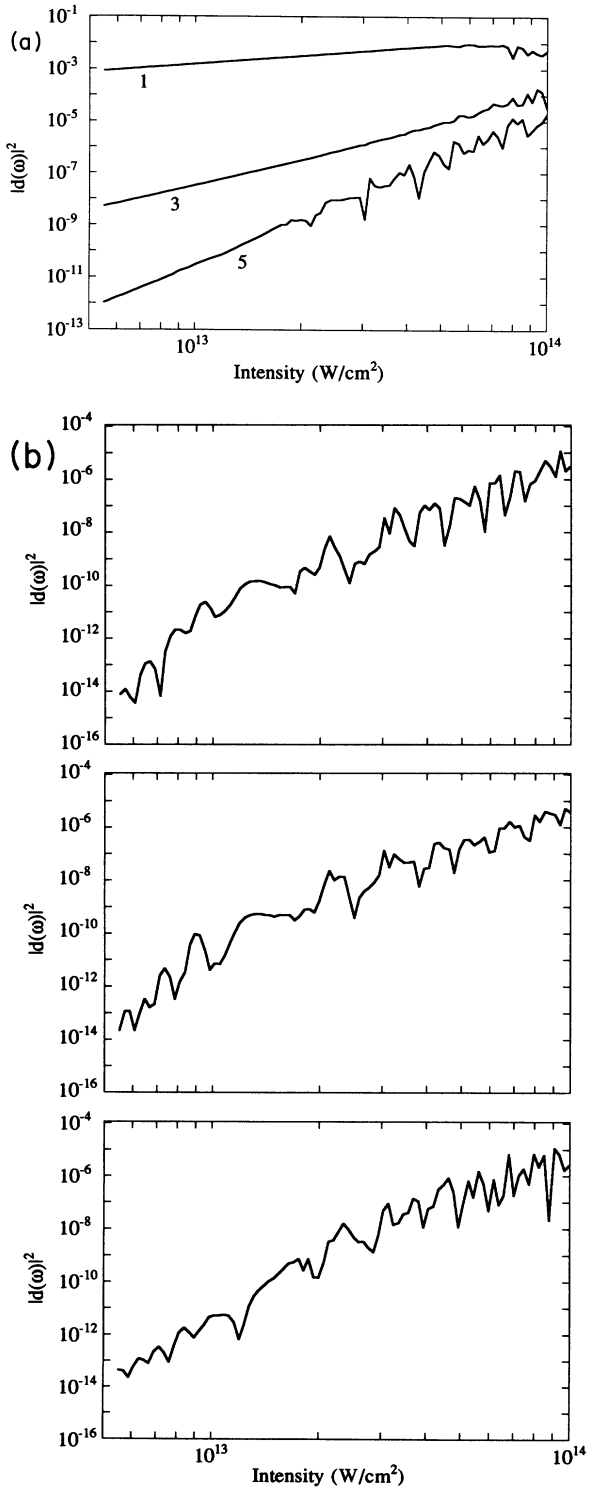

FIG. 8. Intensity dependence of the harmonic radiation for a hydrogen atom at 1064 nm for (a) harmonics 1, 3, and 5 and (b) harmonics 7 (top), 9 (middle), and 11 (bottom).

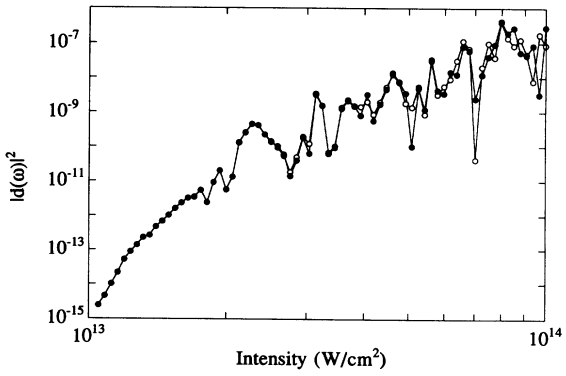

FIG. 9. Intensity dependence of the 19th harmonic for a hydrogen atom at 1064 nm as calculated on a grid of $R=150a_0$ by $L=32$ (filled circles) and $R=225a_0$ by $L=48$ (open circles).

terference than the ionization rate.

Figure 9 shows the intensity dependence of the 19th harmonic as calculated on two grids, one with a dimension of $R=150a_0$ and $L=32$, and the other 50% larger, or $R=225a_0$ by $L=48$. The grids in both calculations were augmented by a $50a_0\cos^{1/8}$ mask function. At intensities up to about $(4-5)\times10^{13}$ W/cm^2, the two calculations agree very well. At higher intensities, as the wave function interacts increasingly with the edges of the grid, the spectra start to diverge, and the results become very sensitive to the "basis" defined by the grid parameters. Small changes in the integration parameters cause the resonances to shift slightly in energy and to display significant variations in amplitude with intensity. This sensitivity is a major complicating factor in calculating high-intensity harmonic spectra. A similar phenomenon occurs, for example, in basis-set-type calculations if one attempts to use a fixed, finite basis to resolve many closely spaced, overlapping scattering resonances.

Figure 10 shows harmonic intensities at 2, 4, 6, 8, and 10×10^{13} W/cm^2, as calculated on a grid of $R=225a_0$ by $L=48$. This figure clearly illustrates the motivation for performing experiments and calculations at high intensities. As the intensity increases, the harmonic intensities also increase, and the plateau extends to higher order. However, as shown in Fig. 11, the background also increases with increasing laser intensity, and eventually begins to interfere with the harmonics. As we discussed above, one of the major contributions to the background is excited-state–to–excited-state ("Raman-like") transitions. Saturating the background requires grids large enough to characterize all of the states important to the dynamics. In the $225a_0$ box, bound states up to about $n=15$ are well resolved on the grid. It is difficult to imagine that states higher than this contribute significantly to the calculations, because population in Rydberg states very close to the ionization potential does not remain in the vicinity of the nucleus. We find that the background level is saturated on the $225a_0$ grid, even at the highest intensities considered. However, a problem that occurs with increasing severity as the intensity increases is reflection from the edges of the grid, which has a definite, observable effect on the spectra. All of the spectra in Figs. 10 and 11 except for 2×10^{13} W/cm^2 show some contribution from reflection, in the form of spurious harmonics. Because these extra harmonics can be as intense as the harmonics in the plateau, it is important to establish their source, and, if possible, to find a way to minimize their effect. We have performed extensive tests to determine which of the harmonics at high intensity are believable and which are not, and to which aspects of the calculation the spurious harmonics are most sensitive. Some indication of how reflection and other numerical artifacts affect the calculated harmonic spectra can be obtained by examining the spatial dependence of the harmonic emission.

As we mentioned previously, at 2×10^{13} W/cm^2 the harmonic spectra are insensitive to the endpoint of the radial integration used to determine $\langle d(t)\rangle$ as long as it is greater than $\sim25a_0$. The same is not true at 1×10^{14}

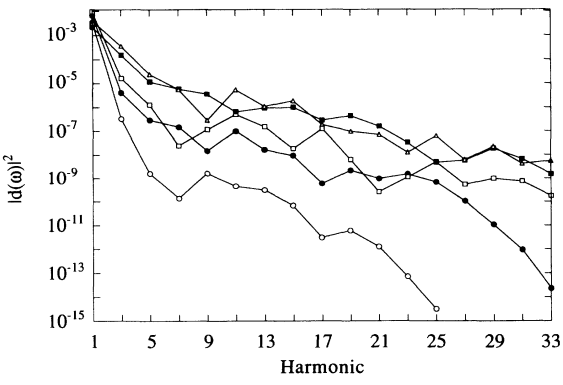

FIG. 10. Harmonic intensities for a hydrogen atom at 1064 nm and laser intensities of 2×10^{13} W/cm^2 (open circles), 4×10^{13} W/cm^2 (filled circles), 6×10^{13} (open squares), 8×10^{13} W/cm^2 (filled squares), and 10×10^{13} W/cm^2 (open triangles).

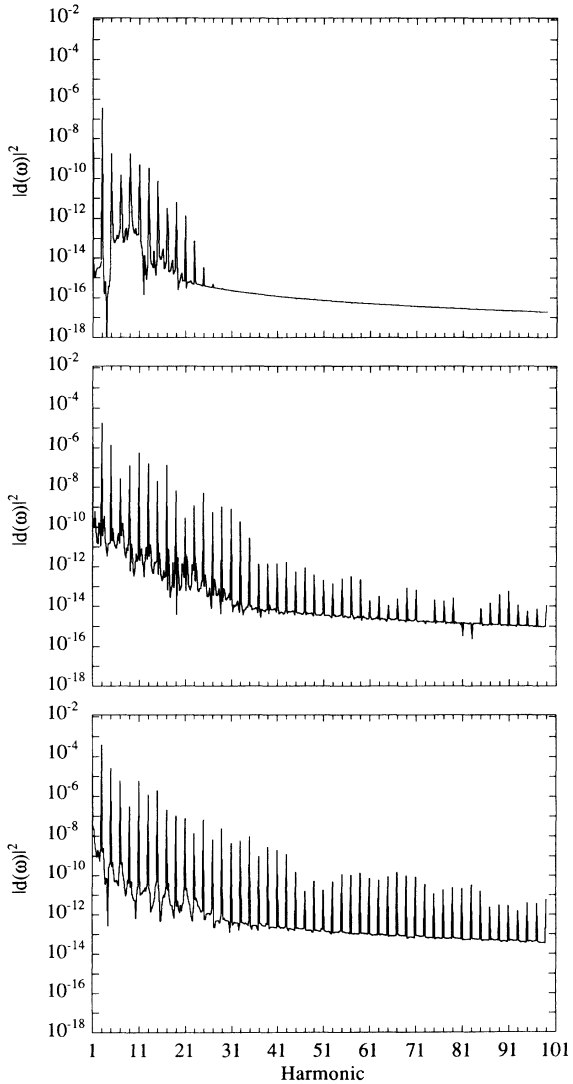

FIG. 11. Harmonic spectra for a hydrogen atom at 1064 nm, and laser intensities of 2×10^{13} W/cm^2 (top), 6×10^{13} W/cm^2, (middle), and 10×10^{13} W/cm^2 (bottom).

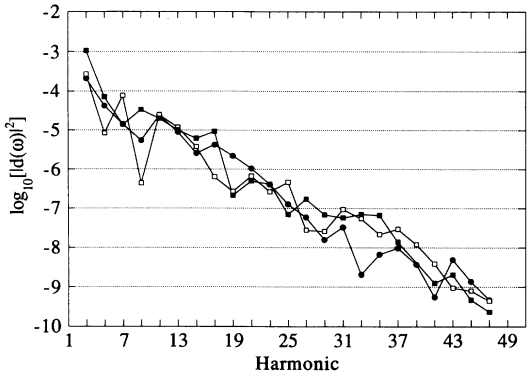

FIG. 12. Harmonic intensities for a hydrogen atom at 1064 nm and 1×10^{14} W/cm^2, calculated on a $1000a_0$ radial grid, with the endpoints of the integration in Eq. (7) set to (filled circles) $150a_0$, (open squares) $250a_0$, and (filled squares) $500a_0$.

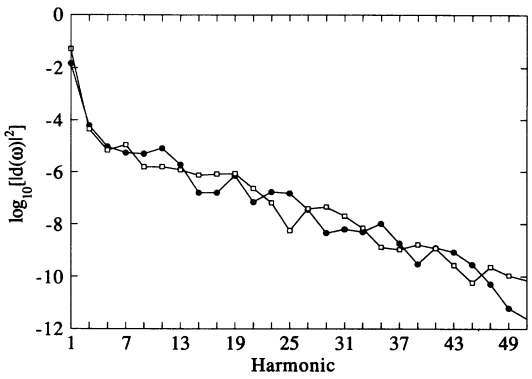

FIG. 14. Contribution to the harmonic intensities for a hydrogen atom at 1064 nm and 1×10^{14} W/cm^2 from (filled circles) $0-50a_0$ and (open squares) $50-250a_0$.

W/cm^2. Figure 12 shows harmonic spectra calculated on a $1000a_0$ grid, with the endpoints of the integration in Eq. (7) set to 150, 250, and $500a_0$. The spectra are quite different. Figure 13 shows the contribution to the harmonic spectra at 2×10^{13} W/cm^2 from 0 to $50a_0$ compared to that from a spherical shell of $50-250a_0$ surrounding the nucleus. As expected, the dominant contribution to the spectrum occurs when the electron is near the nucleus. However, as the intensity increases the contribution to the dipole from regions far from the nucleus gradually increases as well. By 1×10^{14} W/cm^2, as shown in Fig. 14, the contribution to the spectrum from 50 to $250a_0$ is comparable to that from 0 to $50a_0$. This result is problematic, since nonlinear scattering processes should occur only when an electron interacts with a photon near the nucleus, in regions where the potential is changing rapidly. At high intensity, though, a substantial fraction of the wave function has been excited to regions far from the nucleus. The electron executes a quiver motion as it moves away from the nucleus of $\sim60a_0$ at 1×10^{14} W/cm^2, and can continue to serve as a radiation source. A similar effect has been reported in classical simulations [12], where the background completely dominates the spectrum unless the calculation of the dipole omits the portion of the trajectory far from the nucleus. The spectra can also be affected by small amounts of reflected flux rescattering from the nucleus at quite high energy, with unpredictable effects.

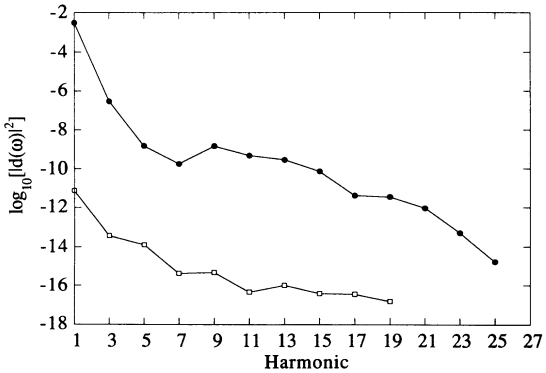

FIG. 13. Contribution to the harmonic intensities for a hydrogen atom at 1064 nm and 2×10^{13} W/cm^2 from (filled circles) $0-50a_0$ and (open squares) $50-250a_0$.

In an attempt to better understand the factors governing the dynamics of harmonic generation, we have employed a simpler, approximate definition of the dipole [28]. This method begins by expanding the wave function in a basis of field-free atomic states,

$$\psi(t)=\sum_m a_m(t)|\phi_m\rangle\ , \tag{12}$$

where the summation is understood to include an integration over continuum states. An equivalent expression for the dipole in Eq. (7) can then be written as

$$d(t)=\sum_{m,n} a_m a_n^*\langle\phi_n|z|\phi_m\rangle\ . \tag{13}$$

If we assume that only the ground-state term is important in the sum, Eq. (13) becomes

$$d(t)\sim\sum_m a_0^* a_m\langle\phi_0|z|\phi_m\rangle+\text{c.c.} \tag{14a}$$

$$\sim a_0^*\langle\phi_0|z|\psi(t)\rangle+\text{c.c.}\ , \tag{14b}$$

where the index zero labels the ground state.

Equation (14) contains only contributions to the dipole from transitions that are directly connected to the ground state. Thus, for example the 19th harmonic is produced only by emission of a photon of 19 $\hbar\omega$ to the ground state. This expression also excludes contributions from regions far from the nucleus by the explicit projection onto ϕ_0, which has a relatively small spatial extent.

We have also repeated a subset of our calculations using the acceleration form of the dipole operator, which can be written as

$$d_A(t)=\left\langle\psi(\mathbf{r},t)\left|\varepsilon_0 f(t)\sin(\omega_0 t)-\frac{z}{r^3}\right|\psi(\mathbf{r},t)\right\rangle\ . \tag{15}$$

The harmonic spectra are then calculated as

$$\sigma(\omega) \propto |d_A(\omega)|^2 = \left| \frac{1}{\omega^2 (T_2 - T_1)} \int_{T_1}^{T_2} dt\, e^{-i\omega t} d_A(t) \right|^2 . \tag{16}$$

Because the operator in Eq. (15) weights the wave function by $1/r^3$, this form of the dipole should also be less sensitive to the behavior of the electron in regions far from the nucleus than the length form.

At low intensities, the spectra produced by all three methods, the length, acceleration, and alternate forms of the dipole, agree quite well. However, at high intensity, the alternate and acceleration forms show far less effects of reflection, and a greatly reduced background. Figures 15 and 16 show harmonic spectra calculated with the three methods at 1×10^{14} W/cm^2. In the plateau region, the intensities agree very well. However, the plateau in the spectrum calculated with the length form extends to much higher order than the plateaus in the spectra calculated with the other two methods. We believe that the extra harmonics in the length-form spectra are spurious, and are due to the interaction of the wave function with the boundary. The spectra calculated with the acceleration and alternate forms are in excellent agreement at the cutoff. Some evidence of reflection remains in these spectra but the spurious harmonics appear after the cutoff and are much lower in intensity. Examining the full spectra in Fig. 16, we see that the overall background levels in the acceleration and alternate forms agree fairly well, and are much lower in magnitude than the length form. The details of the background in the Rydberg region differ in all three spectra. Finally, the intensity dependence of a given harmonic, as shown in Fig. 17 for the 19th harmonic, illustrates that the acceleration and alternate forms tend to agree better with each other than they do with the length form, though the agreement does vary somewhat depending on the harmonic. We note that the 19th harmonic is one of the more difficult to converge in this intensity range because the Rydberg states have been ac Stark shifted to near the energy of the harmonic. All three forms continue to show strong effects of resonances, and individual harmonics that are unusually sensitive to the parameters of the calculations.

Comparison of the three different ways to calculate the dipole moment tends to support the conjecture that the background in the length form is due primarily to contributions to the dipole from regions far from the nucleus. The fact that the acceleration and alternate forms have such similar cutoffs is an indication that the background in the length form is unphysical, and that the main result of exciting the electron away from the nucleus is to produce numerical noise. The agreement between the alternate [Eq. (14)] and the acceleration [Eq. (15)] forms gives us confidence that the calculated spectra are converged to within an order of magnitude, and that the sources of the high-order harmonics are transitions that are dipole connected to the ground state. However, if the effects of

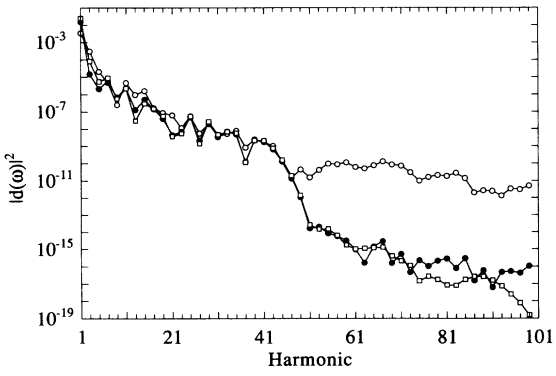

FIG. 15. Harmonic intensities for a hydrogen atom at 1064 nm and 1×10^{14} W/cm^2 as calculated with the length (open circles), acceleration (open squares), and alternate (filled circles) forms of the dipole operator. See the text for the definition of the "alternate" form.

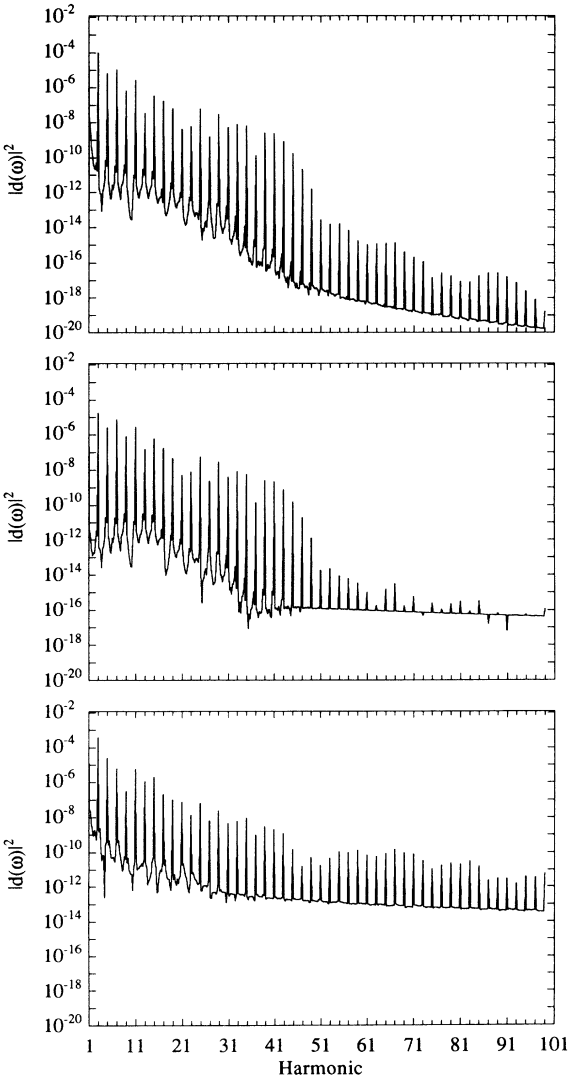

FIG. 16. Harmonic spectra for the same conditions as Fig. 15, for the acceleration (top), alternate (middle), and length (bottom) forms of the dipole operator.

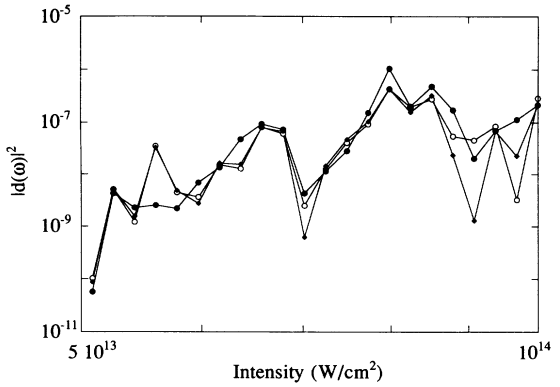

FIG. 17. Intensity of the 19th harmonic for a hydrogen atom at 1064 nm as calculated with the length (open circles), acceleration (filled diamonds), and alternate (filled circles) forms of the dipole operator.

transitions among high-lying Rydberg levels, visible as the structure in the background, are important to the dynamics, the alternate form, which does not include such transitions, will be incorrect, and the acceleration form may be difficult to converge.

IV. CONCLUSIONS

We have shown in this paper that calculating optical harmonic spectra with a nonperturbative, time-dependent method works quite well at intensities at which the wave function is ionizing slowly. The calculations become extremely demanding and difficult as the intensity increases to the point that appreciable ionization occurs during an optical cycle. Harmonic spectra span many orders of magnitude in intensity, and the very high harmonics derive from the dynamics of an extremely small fraction of the wave function. One of our primary purposes in this paper was to show that great care must be taken to calculate harmonic spectra properly if the results are to have even qualitative value.

If the laser intensity is low enough, as it is at 2×10^{13} W/cm^2, most of the electron density remains reasonably close to the nucleus, and converged calculations of manageable size are possible. Even at this intensity, however, the grids required are much larger than those expected from ionization rate calculations. In particular, the grid must be large enough to assure that all of the important excited states are adequately characterized and that the wave function interacts as little as possible with the edges of the grid. Since the calculations are sensitive to even a small amount of reflection, the absorbing boundary must be as efficient as possible.

We showed, by calculating harmonic spectra from a Yukawa potential with one bound state, and a Coulomb potential on an inadequate grid, that excited states contribute to the background radiation and enhance harmonic emission. However, the number of bound states on the grid does not significantly alter the overall number of harmonics. High harmonic emission requires a nonzero matrix element from a virtual bound level or continuum level back to the ground state. This matrix element derives amplitude from the mixing of the bound states, which contain most of the oscillator strength in the atom, into the continuum by the laser field. The cutoff in the spectrum occurs at energies which are too high to have sufficient oscillator strength to emit a photon to the ground state [29].

At 1×10^{14} W/cm^2, the highest intensity analyzed in this paper, the grid required to completely contain the ionizing wave function is enormous, and the wave function in any calculation is interacting strongly with the edges of the grid. As a result, using the length form of the dipole we were unable to obtain fully converged results at this intensity, even on a grid of $2000a_0$, a distance well in excess of the average interatomic spacing in a typical OHG experiment. At such intensities, the results are also very sensitive to small changes in the parameters of the calculation. This situation is akin to the attempt to resolve many narrow, closely spaced scattering resonances with an inadequate basis. Small variations in the basis cause the resonances to shift and interfere unpredictably. At 1×10^{14} W/cm^2, the harmonic spectrum contains contributions from many resonances and many interfering paths, and the harmonics intensities oscillate rapidly as a function of the laser intensity.

Some of the difficulties at high intensity are apparently alleviated by using either an alternate form of the dipole that includes only transitions to the ground state, or the acceleration form of the dipole. The alternate expression is intuitively appealing, because it contains only the term that is expected to dominate harmonic generation. It also diminishes the effects of reflection, which are purely numerical artifacts. The background levels and the cutoffs in the harmonic spectra calculated with the alternate form of the dipole agree quite well with those using the acceleration form of the dipole operator. These results indicate that the length form of the dipole should not be used in high-intensity calculations.

Finally, we would like to emphasize that all of the calculations presented in this paper concern the response of a single atom to a laser field. To compare these results with experiment, the phases and magnitudes of all of the atoms in a macroscopic volume of gas must be combined to predict the experimentally observed signal. This requires knowledge of such parameters as the focal geometry of the laser, and the density, active length, and extent of ionization of the medium. Calculations on xenon have shown [7] that when the highly oscillatory single-atom spectra, such as those in Figs. 8 and 9, are phase matched, the intensity dependence of the harmonics becomes much smoother, in agreement with experiment. The phase-matching results suggest that the most reasonable way to provide single-atom spectra for input to comparisons between theory and experiment is to choose the best grid and mask function possible (given the available computational resources), and then to use the *same* parameters for every intensity. In this way the resonances are treated consistently for all intensities. Our experience indicates that as long as the grid size is at least a few times the quiver motion of the electron, this procedure yields phase-matched harmonic intensities that are in error by no more than an order of magnitude [7].

We are exploring a number of possible ways to improve our calculations, including the use of alternative propagators that may require fewer steps per optical cycle and the transformation to different coordinate systems or gauges. Although the quantity $d(t)$ is gauge independent, it is possible that more efficient absorbing boundaries can be constructed in alternative gauges. We are also examining the recent suggestion [30] that performing the calculations along a complex exterior contour allows flux reaching the grid boundary to be removed analytically. Finally, we have extended these calculations to study harmonic generation in the hydrogen molecule, based on a prediction that molecules should be more efficient than atoms at generating high harmonics [31].

ACKNOWLEDGMENT

This work was performed under the auspices of the U.S. Department of Energy at Lawrence Livermore National Laboratory under Contract No. W-7405-ENG-48.

[1] A. McPherson, G. Gibson, H. Jara, U. Johann, T. S. Luk, I. A. McIntyre, K. Boyer, and C. K. Rhodes, J. Opt. Soc. Am. B **4**, 595 (1987).
[2] A. L'Huillier, L. A. Lompré, G. Mainfray, and C. Manus, in *Multiphoton Processes,* edited by G. Mainfray and P. Agostini (CEA Saclay, France, 1991), p. 45.
[3] N. Sarukura, K. Hata, T. Adachi, and R. Nodomi, Phys. Rev. A **43**, 1669 (1991).
[4] J. F. Reintjes, *Nonlinear Optical Parametric Processes in Liquids and Gases* (Academic, Orlando, 1984).
[5] X. F. Li, A. L'Huillier, M. Ferray, L. A. Lompré, and G. Mainfray, Phys. Rev. A **39**, 5751 (1989).
[6] B. W. Shore and K. C. Kulander, J. Mod. Opt. **36**, **36**, 857 (1989).
[7] A. L'Huillier, K. J. Schafer, and K. C. Kulander, Phys. Rev. Lett. **66**, 2200 (1991); J. Phys. B **24**, 3165 (1991).
[8] B. W. Shore and P. L. Knight, J. Phys. B **20**, 413 (1987).
[9] J. H. Eberly, Q. Su, and J. Javanainen, Phys. Rev. Lett. **62**, 881 (1989).
[10] R. M. Potvliege and R. Shakeshaft, Phys. Rev. A **40**, 3061 (1989); M. Dörr, R. M. Potvliege, and R. Shakeshaft, J. Opt. Soc. Am. B **7**, 433 (1990).
[11] R. A. Sacks and A. Szöke, Phys. Rev. A **40**, 5614 (1989); R. A. Sacks and A. Szöke, J. Opt. Soc. Am. B **8**, 1987 (1991).
[12] G. Bandarage, A. Maquet, and J. Cooper, Phys. Rev. A **41**, 1744 (1990).
[13] K. C. Kulander and B. W. Shore, Phys. Rev. Lett. **62**, 524 (1989); J. Opt. Soc. Am. B **7**, 502 (1990).
[14] K. J. LaGattuta, Phys. Rev. A **41**, 5110 (1990).
[15] P. L. DeVries, J. Opt. Soc. Am. B **7**, 517 (1990).
[16] K. C. Kulander, Phys. Rev. A **35**, 445 (1987).
[17] M. Hermann and J. A. Fleck, Phys. Rev. A **38**, 6000 (1988).
[18] K. J. Schafer, Comput. Phys. Commun. **63**, 427 (1991).
[19] R. S. Varga, *Matrix Iterative Analysis* (Prentice Hall, Englewood Cliffs, NJ, 1962).
[20] S. E. Koonin, K. T. R. Davies, M. Maruhn-Rezwani, H. Feldmeier, S. J. Krieger, and J. W. Negele, Phys. Rev. C **15**, 1359 (1977).
[21] K. C. Kulander, K. R. Sandhya Devi, and S. E. Koonin, Phys. Rev. A **25**, 2968 (1982).
[22] J. K. Crane, M. D. Perry, R. W. Falcone, K. S. Budil, R. Gonzales, and K. Haney (unpublished).
[23] K. J. Schafer and K. C. Kulander, Phys. Rev. A **42**, 5794 (1990).
[24] B. Sundaram and P. W. Milonni, Phys. Rev. A **41**, 6571 (1990).
[25] See, for example, E. Kyrölä, J. Opt. Soc. Am. B **1**, 737 (1984); P. B. Corkum, C. Rolland, and T. Srinivasan-Rao, Phys. Rev. Lett. **57**, 2268 (1968); M. V. Federov, M. Ya. Iranov, and P. B. Lerner, J. Phys. B **23**, 2505 (1990).
[26] L. V. Keldysh, Zh. Eksp. Teor. Fiz. **47**, 1945 (1964) [Sov. Phys. JETP **20**, 1307 (1965)].
[27] C. Pan, K. T. Taylor, and C. W. Clark, Phys. Rev. Lett. **61**, 2673 (1988); J. Opt. Soc. Am. B **7**, 509 (1990); C. W. Clark (private communication).
[28] J. H. Eberly, Q. Su, and J. Javanainen, J. Opt. Soc. Am. B **6**, 1289 (1989).
[29] K. J. Schafer, J. L. Krause, and K. C. Kulander, Int. J. Nonlinear Opt. Phys. (to be published).
[30] C. W. McCurdy and C. K. Stroud, Comput. Phys. Commun. **63**, 323 (1991).
[31] J. L. Krause, K. J. Schafer, and K. C. Kulander, Chem. Phys. Lett. **178**, 573 (1991).